Object-detecting deep learning for mechanism discernment in multi-redox cyclic voltammograms

Benjamin B. Hoar,[1,†] Weitong Zhang,[2,†] Yuanzhou Chen,[2,†] Jingwen Sun,[1] Hongyuan Sheng,[1] Yucheng Zhang,[3] Jenny Y. Yang,[4] Cyrille Costentin,[5,*] Quanquan Gu,[2,*] Chong Liu[1,6,*]

[1] Department of Chemistry and Biochemistry, University of California Los Angeles, Los Angeles, California 90095, United States

[2] Department of Computer Science, University of California Los Angeles, Los Angeles, California 90095, United States

[3] The Oden Institute for Computational Engineering and Sciences, The University of Texas at Austin, Austin, Texas, 78712, United States

[4] Department of Chemistry, University California Irvine, Irvine, California 92697, United States

[5] Université Grenoble-Alpes, DCM, CNRS, 38000 Grenoble, France.

[6] California NanoSystems Institute, University of California Los Angeles, Los Angeles, California 90095, United States.

* Correspondence to: cyrille.costentin@univ-grenoble-alpes.fr (C.C.); qgu@cs.ucla.edu (Q.G.); chongliu@chem.ucla.edu (C.L.)

† Denotes equal contribution

ABSTRACT: In electrochemical analysis, mechanism assignment is fundamental to understanding the chemistry of a system. The detection and classification of electrochemical mechanisms in cyclic voltammetry set the foundation for subsequent quantitative evaluation and practical application, but are often based on relatively subjective visual analyses. Deep-learning (DL) techniques provide an alternative, automated means that can support experimentalists in mechanism assignment. Herein, we present a custom architecture based on Faster R-CNN (Regional Convolutional Neural Network), dubbed as EchemNet, capable of assigning both voltage windows and mechanism classes to electrochemical events within multi-redox cyclic voltammograms. The developed technique detects over 96% of all electrochemical events in simulated testing data and shows a classification accuracy of up to 97.2% on redox events with 8 known mechanisms. Further, the overall inference F_1 score, a combined measure of accuracy and sensitivity in statistical analysis, achieves 0.937, relaying high reliability for detecting and classifying all electrochemical events within complicated voltammograms. This newly developed DL model, the first of its kind, proves the feasibility of redox-event detection and electrochemical mechanism classification with minimal a priori knowledge. The DL model will augment human researchers' productivity and constitute a critical component in a general-purpose autonomous electrochemistry laboratory.

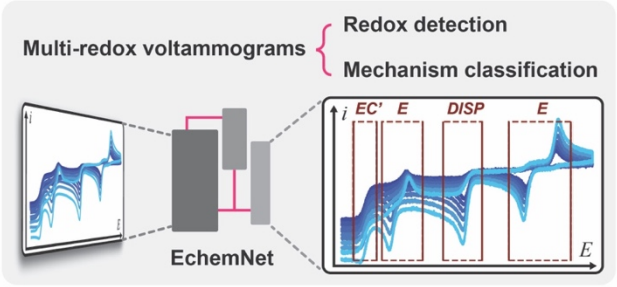

INTRODUCTION

Cyclic voltammetry is one of the most popular analytical electrochemical techniques. [1-4] In fact, there is no need to look beyond the cover of many electrochemistry textbooks to see the famous "duck-shaped" plots of cyclic voltammograms. [2-5] The relationship between current density (i) and applied potential (E) as a function of multiple, n-numbered scan rates (v), represented as $\{v, i(E)\}_n$, is necessary for a descriptive identification of reaction mechanisms with z-numbered redox events, in which each includes the combinations of electrochemical (E_{step}) and possibly chemical (C_{step}) reaction steps. [2, 3, 6] Such a mechanistic identification is a prerequisite for downstream quantitative analyses hence the extraction of thermodynamic and kinetic information within reaction steps. [7] Despite voltammetry's foundational place in the pantheon of electroanalytical tools, there is no consistent heuristic of visual inspection for voltammograms' use in mechanism assignment – perhaps the most common use of cyclic voltammetry. [8] Manual visual inspection of the scan rate's influence on voltammetric responses under different chemical concentrations remains the primary means of mechanism assignment. Reliance on manual inspection precludes any application in high-throughput systems, limits its utility for both experts and non-experts, and renders analysis intractable when cyclic voltammograms increase in complexity and noise. [8-10]

Recent advances in machine learning and artificial intelligence offer a new perspective on voltammogram inspection and mechanism assignment. [8-10] Machine-learning techniques have been applied to mechanistic classification of single-redox voltammograms, [11-13] and numerical fitting of voltammogram data under a pre-determined mechanistic assignment. [14-16] It is proposed that machine learning's expertise in pattern recognition and feature extraction[17] is complementary if not substitutive to manual inspection of electrochemical

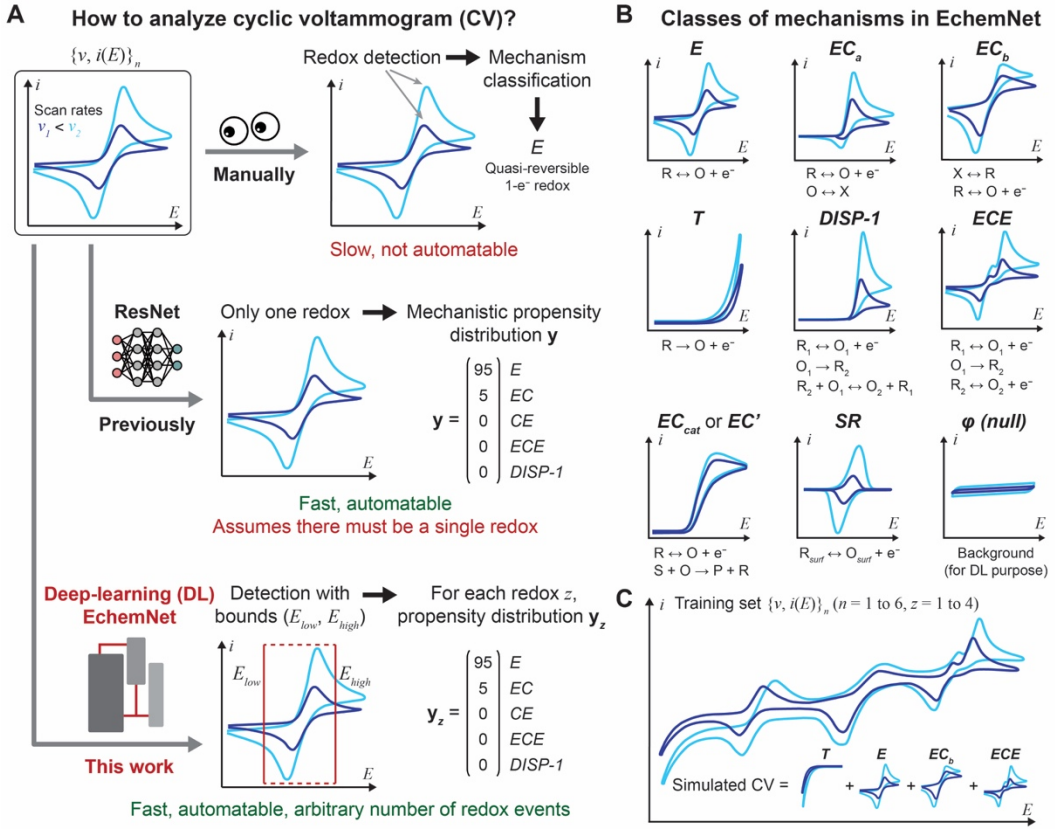

Figure 1. A, the comparison of different approaches to the analysis of cyclic voltammograms (CVs), including the deep-learning (DL) architecture based on Faster R-CNN (Regional Convolutional Neural Network) dubbed as EchemNet. **B**, the classes of electrochemical mechanisms included in EchemNet. **C**, exemplary illustration of simulated multi-redox CVs used as training set in this study. Each data point in the training set contains a set of multi-redox CVs with n-numbered scan rates and z-numbered redox events ($\{v, i(E)\}_n$, n = 1 to 6; z = 1 to 4). ResNet, Residual neural network.

data. [11, 12, 18] For example, our recent work reported a deep-learning (DL) model based on the architecture of ResNet (Residual Neural Network) [19] that automatically analyzes cyclic voltammograms (Fig. 1A), assuming the presence of only one redox event, and designates the probable mechanism among five of the most common ones in homogeneous molecular electrochemistry. [12] The ResNet model yields a probability distribution for five mechanisms, represented as a vector $\mathbf{y} = \{y_i\}$ (i = 1 to 5) in which y_i refers to the mechanistic propensity of the i-th mechanism. Such a probability-driven analysis provides a more satisfying accommodation given the finite amount of available electrochemical data and the finite measurement resolutions of instrumentations. We envision that the deployment of DL-based analysis algorithm not only heralds automated electrochemical analysis with high data throughput, but also opens the opportunities of simultaneous data analysis for multiple electrochemical techniques, a feat untenable by humans owing to the data's nature of high dimensionality. [8]

However, to date, the developed machine-learning models all require one piece of important *a priori* information, namely that the number of redox event z is presumably known (z = 1 in previous reports[11-13]), which renders the DL models not entirely on par with manual inspection. In a typical manual inspection of voltammograms without any *a priori* information, human researchers first identify and locate any redox events in the voltammogram, *i.e.* a task of object detection, then determine the mechanism type for each redox event, *i.e.* a task of classification, before potentially establishing any correlation among redox events in search of causality. While reported algorithms are capable of mechanistic classification for single-redox events in voltammograms, [11-13] a DL algorithm, tasked with both object detection and classification, remains to be developed for automated analysis of cyclic voltammetry. As DL architecture such as Faster R-CNN (Regional Convolutional Neural Network) [20] has been widely used for the recognition and classification of two-dimensional images in a wide range of applications, we envision using Faster R-CNN architecture to develop a voltammogram-reading DL model with the functionalities of both redox-event detection and mechanism classification.

Here we report a custom-designed DL architecture based on Faster R-CNN, the first of its kind and dubbed as EchemNet, capable of both redox-event detection and mechanism classification for multi-redox cyclic voltammograms with minimal *a priori* information (Fig. 1A). As voltammetry data $\{v, i(E)\}_n$ are intrinsically sets of one-dimensional (1D) vectors instead of two-dimensional images, a custom-designed model of 1D Faster R-CNN architecture is developed to locate the potential window for up to 4 redox events ($z \leq 4$) and designate the probable mechanism in a probabilistic manner (Fig. 1A). The EchemNet is trained by simulated multi-redox voltammograms of up to 6 scan rates and up to 4 independent redox events ($\{v, i(E)\}_n$, n = 1 to 6; z = 1 to 4), categorized in 8 different reaction mechanisms spanning homogeneous, heterogeneous, and surface electrochemistry (Fig. 1B). The DL model exhibits an overall F_1 score, a statistical combined measure of binary classification in accuracy and sensitivity, [21] of up to 0.937 towards redox-event detection and mechanism classification among simulated voltammograms, while preliminary testing with experimental data are satisfactory as well. Our work showcases the feasibility of a DL algorithm for voltammogram analysis without the need for any *a priori*

knowledge, hence the genesis of a general-purpose autonomous platform of electrochemical research that augments the productivity of human researchers.

RESULTS

Training set of multi-redox voltammograms. The dataset that yields EchemNet includes simulated multi-redox voltammograms, conducted via finite-element methods using COMSOL Multiphysics v5.5 (Supplementary Note 1). What we sought is to establish a dataset of simulated voltammograms that sample the majority of if not the whole numerical parameter space for each mechanism as defined in textbooks[2, 3] (Supplementary Note 2). Each data point in the dataset includes voltammograms of up to 6 scan rates and up to 4 redox events ($\{v, i(E)\}_n$, n = 1 to 6; z = 1 to 4). 8 common mechanisms in electrochemistry (Fig. 1B) have been included following the textbook definitions (Supplementary Note 3):[2, 3] (1) the single-electron quasi-reversible homogeneous electron transfer (*E*); (2) a single-electron quasi-reversible homogeneous oxidative electron transfer followed by a chemical reaction of the oxidant in the solution (EC_a); (3) a single-electron quasi-reversible oxidative electron transfer preceded by a chemical reaction of the reductant in the solution (EC_b, the anodic variant of the classical *CE* mechanism in Savéant's textbook[3] that is the counterpart of EC_a); (4) the single-electron heterogeneous electron transfer following the Tafel kinetics (*T*); (5) the two-electron homogeneous electron transfer, in which a single-electron transfer is followed by an irreversible chemical and a disproportionation steps (*DISP-1*); (6) a similar two-electron homogeneous electron transfer, in which a single-electron transfer is followed by an irreversible chemical step and a thermodynamically less demanding single-electron transfer (*ECE*); (7) the homogeneous electrocatalysis, in which a single-electron transfer is followed by a chemical step that regenerates the redox-active catalyst (EC_{cat} or *EC'*); (8) the interfacial single-electron transfer when the redox species follows the Butler-Volmer kinetics and is bound on the electrode surface (*SR*). Here the categorization of EC_a and EC_b mechanisms, instead of the classical *EC* and *CE* ones in textbooks[2, 3], is because an anodic/cathodic *EC* mechanism is mathematically equivalent to a cathodic/anodic *CE* one, respectively.

A multi-step process is developed to establish the dataset of simulated multi-redox voltammograms. First, the parameter space of each mechanism, for example the value ranges for scan rate (v), exchange current density (i_0), equilibrium constant (K), and forward kinetic rate constant (k_f) in the EC_a mechanism, is carefully defined following textbooks and prior literature[2, 3] (Table S1, Supplementary Note 3). Second, we randomly sampled about 3,000 parameter combinations following the constraints defined in Table S1, for each mechanism type with up to 6 different scan rates (n = 1 to 6). Third, from the available 8 mechanisms and about 24,000 (= 8 × 3000) parameter combinations, we randomly selected no more than 4 parameter combinations (z = 1 to 4) and deployed finite-element simulations to yield simulated multi-redox voltammograms, with randomized redox sequences, voltage spacings among every redox event, and relative concentrations of redox species that dictate the current densities i among different redox features (Fig. 1C). While in principle there could be about ${}_{24,000}P_4 \sim 10^{17}$ different permutations, about 80,000 data points of simulated multi-redox 6-scan voltammograms ($\{v, i(E)\}_n$, n = 6; z = 1 to 4), about 480,000 (= 6 × 80,000) voltammograms in total, were generated, among which 90% of these data points are the training data and the rest 10% are the test data (Supplementary Note 1). As shown below, such a relatively small amount of data is sufficient for the DL model's establishment.

As we aim to demonstrate the DL's feasibility in analyzing multi-redox voltammograms first, the voltammograms in the proof-of-concept training set assume that each redox event is independent to each other (Supplementary Note 2). We also ensure that the training set includes well-separated redox peaks, and the current densities of redox peaks are on the same order of magnitudes among all redox events (Supplementary Note 4). As the training of object detection algorithm requires the "ground truth" of the location for each redox event, a custom protocol is implemented to yield the voltage window, presented as the cathodic and anodic voltage bounds (E_{low} and E_{high}, respectively), for each redox event in the simulated voltammogram (Supplementary Note 4). The use of E_{low} and E_{high} to represent the voltage window without information of current density i is consistent with our design of one-dimensional (1D) object-detection model (see below). Last, a certain extent of Gaussian noise, with a dimensionless standard deviation $\sigma_{train} = \sigma_{test} = 0.01$ unless otherwise noted, was applied to the normalized current density $i_{normalized}$ (Supplementary Note 5) following the same protocol as our previous work.[12] The voltammogram data $\{v, i(E)\}_n$ and the corresponding ground truth E_{low} and E_{high} were normalized before being deployed for the model's training, validation, and testing (Supplementary Note 5).

Design of deep-learning (DL) architecture. A custom-designed Faster R-CNN architecture was needed to establish the EchemNet model. The presence of multiple electrochemical mechanisms within a single cyclic voltammogram precludes the use of image classification algorithms such as ResNet[19] alone. Alternatively, convolutional layer-based algorithms, specifically object detection algorithms, can be considered as a mature technology for the elucidation of electrochemical mechanisms contributing to a convoluted $\{v, i(E)\}_n$ output. One such architecture, Faster R-CNN,[20] is selected for three reasons: (1) its online region proposal network (RPN) enables end-to-end training on detection and classification tasks; (2) the deployment of feature pyramid networks[22] promotes multi-scale detections; (3) the architecture's alignment algorithm of region of interest (RoI), generated from RPN, provides generally high fidelity between known and predicted event bounds – in our case the voltage windows (E_{low} and E_{high}) containing redox events. However, although typical algorithms of Faster R-CNN are developed for the analysis of two-dimensional (2D) images,[20] object detection in voltammograms is intrinsically a one-dimensional (1D) task, because from chemistry perspective the location of every redox event should only be *E*-dependent in voltammograms. A deployment of 2D RoI in voltammograms will explicitly introduce the magnitude of current density i as a criterion of redox-event detection, inadvertently position a bias towards large redox events and significantly decrease the detection sensitivity towards small ones. Therefore, the intrinsic feature of voltammograms, and more broadly electrochemical data in general, calls for a 1D adaptation of the DL architecture.

Hence, we employed the tools in Faster R-CNN with the custom implementation of a 1D RPN and 1D RoI align algorithm to obtain a highly effective means of mechanism enumeration from complex voltammogram data (Fig. 2A and S1, Supplementary Note 5). In typical 2D image recognition, the algorithm evaluates the performance of object detection with the term named as Intersection over Union (IoU), which is calculated as the ratio of the overlap area ("Intersection") to the

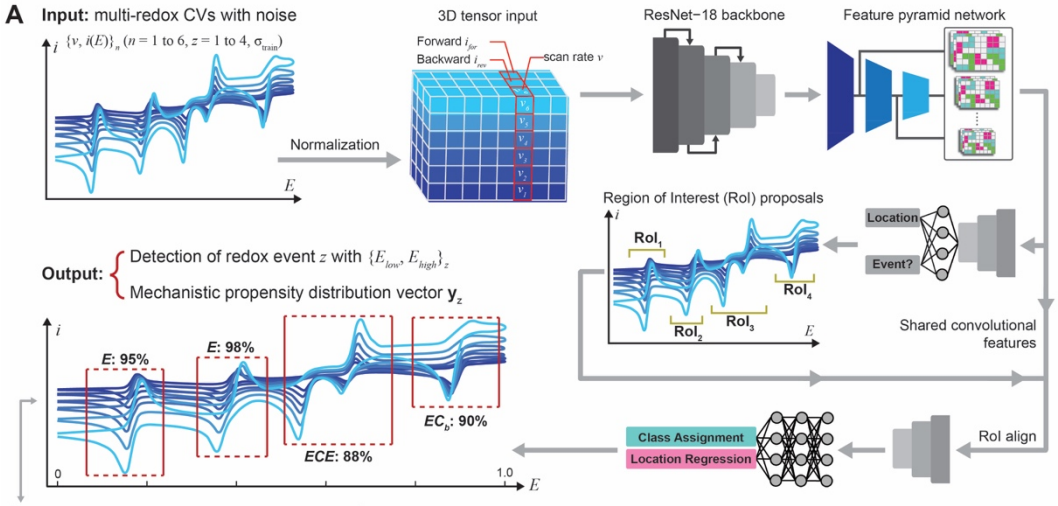

$\mathbf{y}_z$ (z = 1 to 4)	RoI$_1$	RoI$_2$	RoI$_3$	RoI$_4$
E_{low} (normalized)	0.065	0.313	0.508	0.795
E_{high} (normalized)	0.237	0.470	0.749	0.989
E (100%)	94	98	1	7
EC_a (100%)	5	2	3	0
EC_b (100%)	0	0	2	90
T (100%)	0	0	0	0
DISP-1 (100%)	1	0	6	1
ECE (100%)	0	0	88	0
EC_{cat} (100%)	0	0	0	0
SR (100%)	0	0	0	0
φ (100%)	0	0	0	2
Most probable	***E***	***E***	***ECE***	***EC$_b$***

	Ground truth	RoI$_1$	RoI$_2$
E_{low}	0.3	0.6	0.2
E_{high}	0.9	1.1	0.8
IoU	–	0.38	0.86
Good detection?		X	✓

Figure 2. A, The input, output, and general architecture of the deep-learning (DL) model, "EchemNet", tailored to the analysis of multi-redox cyclic voltammograms (CVs). **B**, Highlights in the custom-designed model that includes one-dimensional (1D) regions of interest (RoIs) and the calculation of intersection over union (IoU), in comparison to the default two-dimensional (2D) one used in image recognition. The use of 1D RoI ensures that object detection will not be inadvertently affected by the magnitude of current density i and will not lose sensitivity towards small redox features.

combined area ("Union") between an algorithm-detected object and the corresponding ground truth in a 2D image (hence IoU ∈ [0,1]) (Fig. 2B). In accordance with the 1D adaptation of RPN and RoI, to assess the quality of object detection, 1D IoU was calculated as the ratio of the overlap voltage range to the combined one between algorithm-yielded voltage window (E_{low} and E_{high}) and the corresponding ground truth (IoU ∈ [0,1] as well) (Fig. 2B). The algorithm also deploys ResNet, as reported in our previous work[12], for the classification in each RoI among the aforementioned 8 mechanisms and the null class (φ) that indicates the voltammogram background without any designated redox events (Fig. 1A). As exemplified in Fig. 2A, the developed EchemNet after satisfactory training (Fig. S2) is designed to discern multi-redox voltammograms and enumerate the voltage window of the z-th detected redox event (RoI$_z$) represented as normalized voltage values (E_{low} and E_{high}), the corresponding mechanistic propensity distribution $\mathbf{y}_z = \{y_{z,i}\}$ (i = 1 to 9) towards the trained 8 redox mechanisms plus φ class, and the assignment of the most probable mechanism.

Performance evaluation. There are two separate yet related metrics for the evaluation of a DL model for both object detection and classification: Metric I, the effectiveness of the RPN to detect events independent of their mechanism, *i.e.* performance in object detection alone; Metric II, the overall inference performance which is the combination of object detection (matching of predicted voltage windows with the ground truth) and classification (matching of the predicted most probable mechanism with the ground truth) of the RoIs provided by the RPN (Fig. S1). In the evaluation of object detection alone (Metric I, Fig. 3A), 3 different outcomes are possible through the course of region proposal and object detection: RoIs represented as E_{low} and E_{high} predicted by the RPN could ultimately align with ground truth of redox bounds (object detection true positive, tp_1; IoU ≥ 0.75) or not (object detection false positive, fp_1), and regions where known true redox bounds were not detected were assigned as false negatives (fn). In the evaluation of overall inference performance (Metric II, Fig. 3A), a true positive (tp_2) is logged when the ground truth mechanism i for the z-th detected redox is confidently denoted as the most probable mechanistic propensity in $\mathbf{y}_z$ vector ($y_{z,i} \geq 0.7$) with good overlap with the redox's voltage bounds (IoU ≥ 0.75); while the false positives are further categorized based on whether the model-yielded RoIs detect a real redox event (fp_2) or merely detect φ background (fp_3) (Fig. 2A). There is no delineation between the false negatives (fn) between object detection (Metric I) and overall inference (Metric II), hence the fn sub-population remains the same to the evaluation of object detection and overall inference metrics.

The developed DL model was evaluated for its performance, in a protocol similar to our previous report, [12] after being trained by simulated multi-redox voltammograms ($\{v, i(E)\}_n$, n = 6; z = 1 to 4; σ_{train} = 0.01). The test set for the DL model includes about 8,000 points of 6-scan voltammograms, 10% of the whole dataset, that were not exposed to the developed DL model during the training process. The DL model exhibits an average IoU of 0.966 among the test set, where unity constituted a perfect overlap of predicted bounds with ground truth voltage windows. Following the protocol of statistical analysis in image recognition and more generally binary classification, [21] the

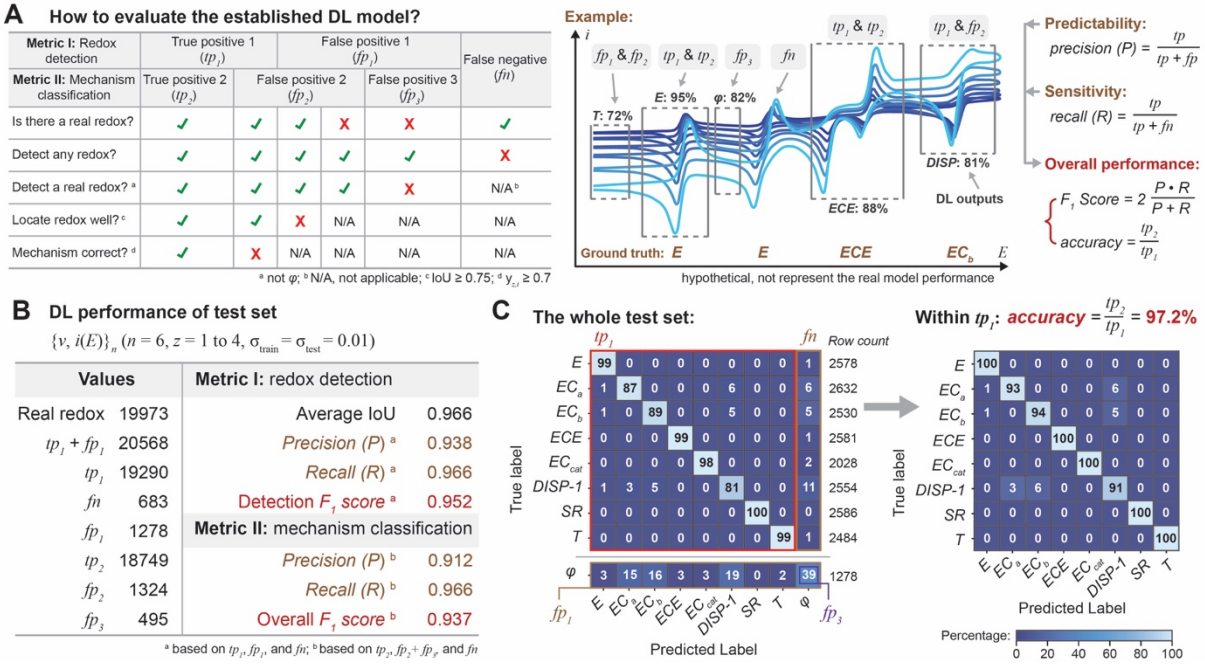

Figure 3. A, Explanations to the true positives, false positives, and false negative in the established EchemNet model for both redox-event detection and mechanism classification, along with the definitions of metrics for performance evaluation. **B**, The assay of test-set voltammograms and the DL model's performance. The test set is roughly 10% of the whole dataset of simulated voltammograms (Supplementary Note 1). **C**, Confusion matrix from the test-set assay for the whole test set (left) and within the cases of true positive 1 (tp_1) after redox-event detection (right). Row count, the number of encounters when the corresponding mechanism on the row of "True label" were analyzed in the test set.

precision (P) and recall (R) of both metrics are calculated to evaluate the predictability and sensitivity, respectively, of the DL model (Fig. 3A). Calculating the harmonic means of P and R in both metrics lead to the F_1 scores, an overall measure of a model's performance[21]. As shown in Fig. 3B, the F_1 scores in Metrics I and II reach 0.952 and 0.937, respectively, illustrating strong performance by the RPN (Metric I) and overall balanced performance with high values of both precision and recall (Metric II). Such a performance is satisfactory to say the least, based on the standard of image recognition, [21] within our aforementioned assumptions and our dataset of simulated voltammograms.

We also evaluated the class-by-class accuracies from the developed EchemNet model. As the developed ResNet classifies RoI into not only the 8 designated electrochemical mechanisms but also the null class (φ), *i.e.* the background without any redox events, we first established a confusion matrix that includes 8 mechanisms and the φ events with tp_1, fn, fp_1, and fp_3 events highlighted (left in Fig. 3C). The number of encounters for each mechanism in the test set ("Row counts" in Fig. 3C) is relatively homogenous among all mechanisms, illustrating a fair and balanced test to the DL model. Practically, the DL's functionality in the context of mechanism classification will not be affected by the presence of fp_1 cases with φ prediction (hence fp_3), contributing to 39% of total fp_1 cases, when the DL algorithm unnecessarily yet correctly identifies a voltage window in the voltammogram that does not have any redox events and can be easily dropped in our model. Therefore, we plotted a revised confusion matrix among all tp_1 cases, with a tp_2 accuracy of 97.2%, presumably better reflecting the model's utility in mechanistic analysis (right in Fig. 3C). Our results suggest that *DISP-1* mechanism is the most confused one, evident from non-negligible probabilities of mis-assigning a *DISP-1* mechanism as EC_a/EC_b, or vice versa. Such phenomenon is similar to the one observed in our previous report of ResNet architecture for mechanism classification when only one redox event is known to exist. [12] The results reflect the similarity in voltammograms among *DISP-1* and *EC/CE* mechanisms, as depicted in the textbooks, [2, 3] when the single-electron (*EC/CE*) and two-electron processes (*DISP-1*) are both under pure kinetic conditions.

Deployment examples. We first illustrate the utility of the developed EchemNet model via analyzing simulated voltammograms. Fig. 4A to 4D display the simulated voltammograms ($\{v, i(E)\}_n$, n = 6, σ_{test} = 0.01) with the number of redox events z = 1, 2, 3, and 4, respectively, which was new to the trained DL model. The solid dark-red rectangles denote the redox events' voltage windows (E_{low} and E_{high}), derived based on our protocol and designated as the ground truth (Supplementary Note 4), while the dashed ones of bright-red color denote the RoIs generated from EchemNet's analysis. The close match between the designated ground truths and the analyzed RoIs suggest satisfactory performance of object detection with a IoU threshold value of 0.75 (tp_1 in Fig. 3A). Moreover, each detected redox event is subject to mechanistic classification via the ResNet architecture. The most probable mechanism for each redox z (RoI_z) is labelled on the voltammograms along with the corresponding propensity $y_{z,i}$, while the DL model outputs the whole $\mathbf{y}_z$ vector of mechanistic propensities. The high $y_{z,i}$ values for the correctly predicted mechanisms illustrate the model's high analytic fidelity. Statistically, our testing of about 8,000 points of simulated 6-scan voltammograms report the tp_2 accuracies of 98.2%, 97.8%, 97.2%, and 96.6%, when z = 1, 2, 3, and 4, respectively. Such results indicate that despite slight decay the tp_2 accuracy is relatively insensitive against the number of redox events (z) and the DL model is robust against the increasing complexity in the voltammograms.

We deployed the EchemNet to analyze experimental data in exemplary chemical systems. Cobalt(II) tetraphenylporphyrin

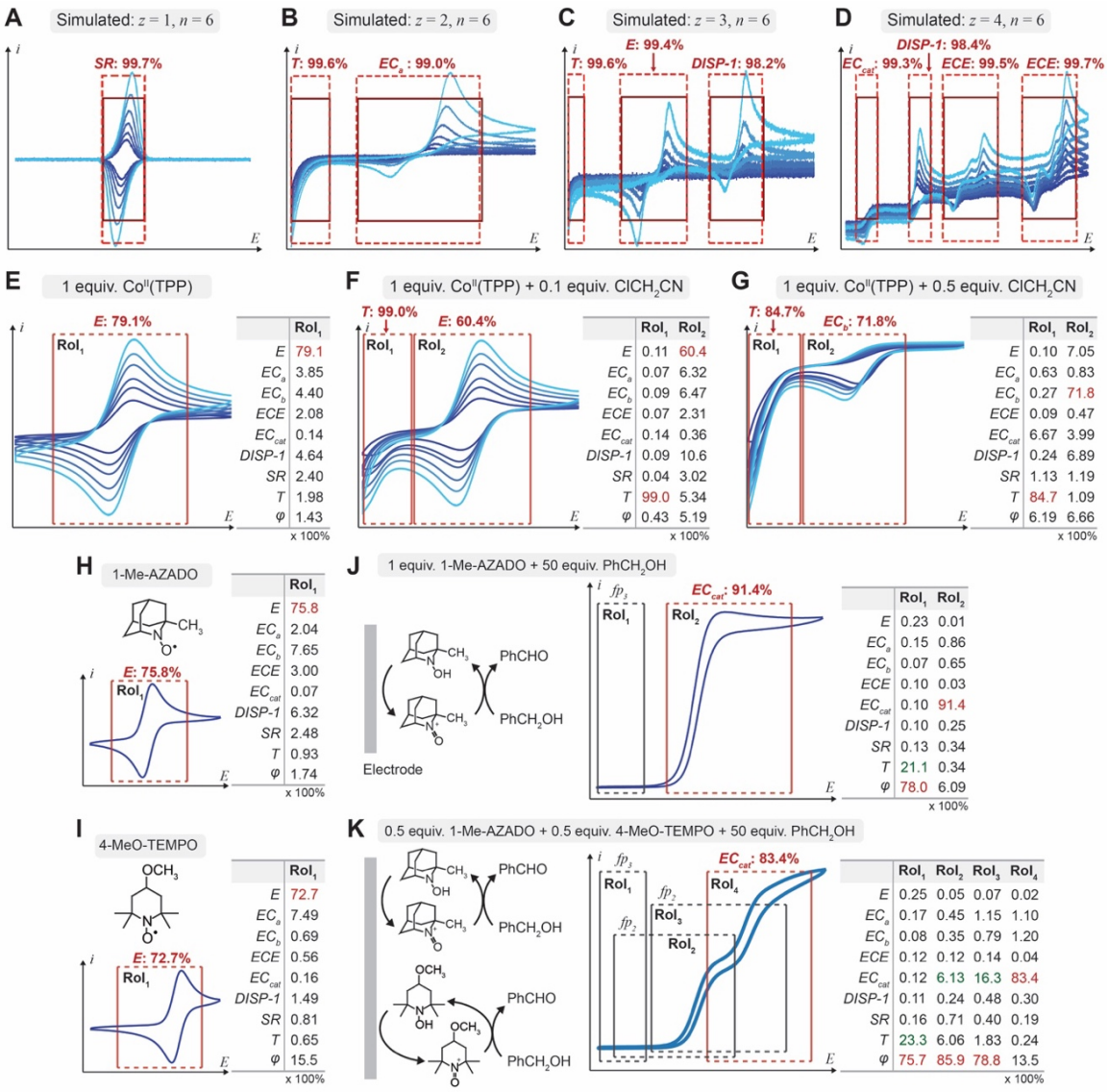

Figure 4. A to **D**, simulated voltammograms of 6 different scan rates ($v = 6$) with 1, 2, 3, and 4 redox events ($z = 1$, 2, 3, and 4), respectively. The most probable mechanisms from the DL model, also the ground truths, are labelled with corresponding propensity values. The solid dark-red rectangles denote the ground truths of redox's voltage windows (E_{low} and E_{high} in Supplementary Note 4), and the dashed ones of bright-red color denotes the DL-generated RoIs. **E** to **G**, experimental voltammograms of 1 mM cobalt(II) tetraphenylporphyrin ($Co^{II}TPP$) alone (**E**), and with 0.1 mM and 0.5 mM chloroacetonitrile ($ClCH_2CN$) (**F** and **G**, respectively). 0.1 M tetrabutylammonium hexafluorophosphate (NBu_4PF_6) in dimethylformamide (DMF); –1.5 V to –0.9 V vs. Ag/10 mM Ag^+ reference electrode; 10, 20, 30, 50, 70, and 100 mV/s; 3rd cycle; *iR* compensated. **H** to **K**, experimental voltammograms of 1 mM 1-methyl-2-azaadamantane-N-oxyl (1-Me-AZADO) alone (**H**), 1 mM 4-methoxy-2,2,6,6-tetramethylpiperidine-1-oxyl (4-MeO-TEMPO) alone (**I**), 1 mM 1-Me-AZADO with 50 mM benzyl alcohol ($PhCH_2OH$) (**J**), and 0.5 mM 1-Me-AZADO and 0.5 mM 4-MeO-TEMPO with 50 mM $PhCH_2OH$. 0.15 M $NaHCO_3/Na_2CO_3$ buffer (pH 9.14); 0.05 to 0.85 V vs. Saturated Calomel Electrode (SCE); 50 mV/s; 3rd cycle; *iR* compensated. The RoIs from EchemNet and the corresponding propensity distribution vectors $\mathbf{y}_z$ towards 8 mechanisms plus background (φ) are all labelled in **E** to **K**. The voltammograms plotted in **E** to **K** have been normalized in both axes so that the exact E and i values are not displayed. More information is available in Supplementary Note 6.

($Co^{II}TPP$) is known to undergo a quasi-reversible one-electron charge transfer (E step) between formally Co(II) and Co(I) redox states (~ −0.785 V vs. Saturated Calomel Electrode, SCE[23]) in dimethylformamide (DMF) (Supplementary Note 6). From experimental voltammograms ($n = 6$), such an E step was correctly detected and classified by the DL model based on both RoI alignment and the corresponding $\mathbf{y}_z$ vector that includes mechanistic propensities of 8 mechanisms plus background (φ) (Fig. 4E). When chloroacetonitrile ($ClCH_2CN$) was added to the solution, the electrogenerated Co(I) species nucleophilically attacks $ClCH_2CN$ electrophile and yields Co(III)−CH_2CN, rendering the Co(II)/Co(I) redox irreversible (EC_b mechanism due to its cathodic nature). At a more cathodic potential (< ~ −1.0 V vs. SCE[23]), the yielded Co(III)−CH_2CN species is reported to undergo multiple steps in a catalytic fashion, yielding voltammogram responses resembling either a T or EC_{cat} mechanism. [23] At a small equivalent of $ClCH_2CN$ (Fig. 4F), the DL model correctly detects and classifies the catalytic process at more cathodic potentials (RoI_1), while detecting the Co(II)/Co(I) redox and classifies it as an E mechanism (RoI_2), albeit with a much lower propensity (y_E = 60.4 % in Fig. 4F against 79.1% in Fig. 4E), consistent with the increase of irreversibility owing to the reaction between Co(I) and $ClCH_2CN$. [23] At a larger equivalent of $ClCH_2CN$ (Fig. 4G), similar catalytic (RoI_1) and Co(II)/Co(I) (RoI_2) features are detected from the voltammograms, yet now the Co(II)/Co(I)

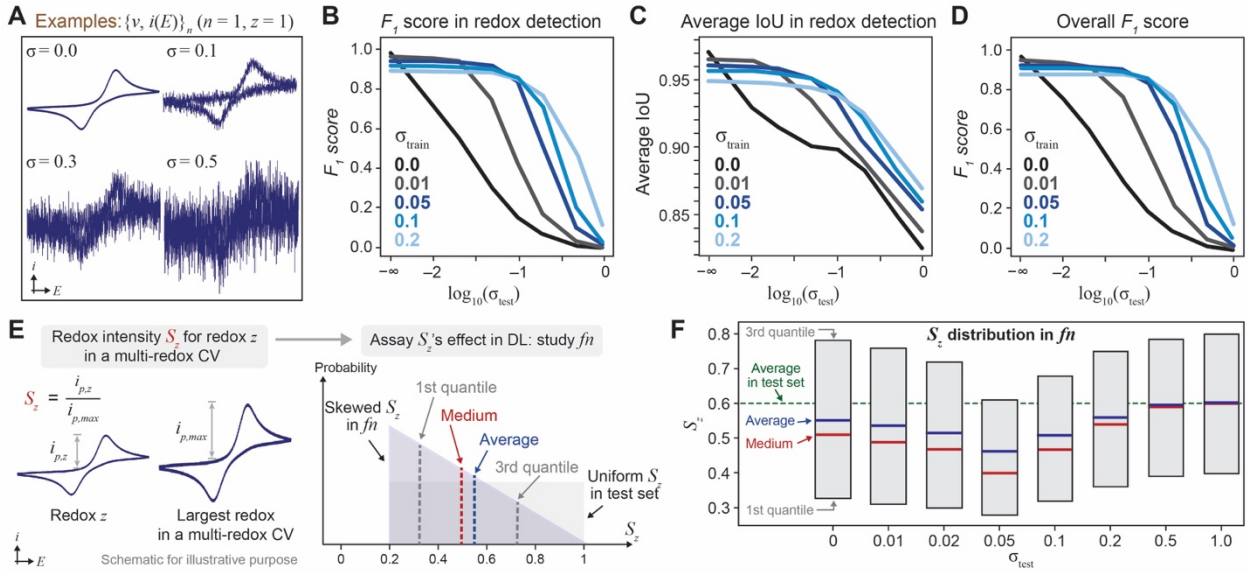

Figure 5. A, Exemplary illustration to showcase how noise (σ) affect CV data quality. **B** to **C**, plots of the F_1 score in redox-event detection (**B**), average IoU value in redox-event detection (**C**), and overall F_1 score from both redox-event detection and mechanism classification (**D**) against the noise in the test set (σ_{test}, [0.0, 1.0]), for DL models developed under different degrees of noise in the training set (σ_{train}, [0.0, 0.2]). $\log_{10}(-\infty) = 0$. **E**, the dimensionless scaling factor S_z of redox z's relative intensity (in terms of current density) against the strongest one within a multi-redox CV, and the comparative analysis of S_z distributions between the test set (a uniform distribution, [0.2, 1.0]) and the *fn* cases from DL. **F**, the S_z distributions in the *fn* cases under different σ_{test} values using the DL model trained by $\{v, i(E)\}_n$ ($n = 6$; $z = 1$ to 4; $\sigma_{train} = 0.01$).

redox is so irreversible that the most probable mechanism is assigned as EC_b (71.8%), indicative a greater extent of the reaction between Co(I) and $ClCH_2CN$. The DL analysis of the electrochemical data for $Co^{II}TPP$ in the presence of $ClCH_2CN$ is satisfactory.

We further challenged the DL model to analyze the redox and catalysis of nitroxyl derivatives in aqueous solutions, [24, 25] but now with only a single voltammogram curve ($n = 1$) instead of the default value of 6 (Supplementary Note 6). This is intended to test whether the DL model, while trained by $\{v, i(E)\}_n$ ($n = 6$), is applicable towards electrochemical dataset with a smaller number of scan rates. As implemented in our prior work, [12] we populated the 3D input tensor with 6 identical voltammograms and scan rates and feed the tensor into the DL model for analysis (Supplementary Note 5). Quasi-reversible redox features of 1-methyl-2-azaadamantane-N-oxyl (1-Me-AZADO) (Fig. 4H) and 4-methoxy-2,2,6,6-tetramethylpiperidine-1-oxyl (4-MeO-TEMPO) (Fig. 4I) are both successfully detected and classified as an *E* mechanism. When benzyl alcohol ($PhCH_2OH$) substrate is added to the solution of 1-Me-AZADO, two-electron electrocatalytic oxidation of $PhCH_2OH$ via the EC_{cat} (or *EC'*) mechanism emerges (Fig. 4J). [3, 24, 25] Such voltammetric response is correctly detected and identified (RoI_2), yet a false positive (fp_3) is also yielded with a 79.0% of φ propensity (RoI_1). When $PhCH_2OH$ are added to a mixture of 1-Me-AZADO and 4-MeO-TEMPO, both 1-Me-AZADO and 4-MeO-TEMPO serve as EC_{cat} electrocatalysts in parallel, albeit at different catalytic onset potentials (Fig. 4K). [24] The resultant voltammogram display a two-step staircase shape, which was not close to any of the scenarios by which the DL model was trained. Surprisingly, the DL model correctly detects and classifies the general trend of the EC_{cat} mechanism (RoI_4), amid one fp_3 (RoI_1) and two fp_2 (RoI_2 and RoI_3) cases with high φ propensities (> 75%) (Fig. 4K). It is interesting that both fp_2 cases correctly detect redox events beyond the background and the second most likely mechanism are both EC_{cat} (6.13% and 16.3%, respectively). Our results suggest that the EchemNet may still be used for voltammograms with fewer scan rates (n < 6), yet prone to false-positive outputs. Practically, the issue of false-positives can be addressed in post-analysis by removing any detections whose φ propensity is larger than a threshold (say, 60% based on Fig. 4J and 4K). Our results hint that the EchemNet could be "stretched" a bit for the analysis of scenarios new to the model, but a more systematic evaluation ought to be conducted in the future.

Robustness and sensitivity towards noises and sizes of redox features. We evaluated the DL model's robustness against noisy data. While the default DL model is trained by simulated voltammograms with $\sigma_{train} = 0.01$, we have established and evaluated multiple DL models whose training sets were applied with $\sigma_{train} = 0.0$, 0.01, 0.05, 0.1, and 0.2. Exemplary illustrations about how noise σ affect data quality are showcased in Fig. 5A and Fig. S3. Those models' performances against the extent of noise in voltammograms were systematically tested by sets of simulated voltammograms with varying degrees of Gaussian noises ($\sigma_{test} \in [0.0, 1.0]$) and evaluated via the F_1 score of object detection (Metric I) (Fig. 5B), the average IoU values (Metric I) (Fig. 5C), and the overall F_1 score (Metric II) (Fig. 5D). The analysis suggests that the model with $\sigma_{train} = 0.0$ is not noise-robust at all and the performance decreases sharply as σ_{test} increases. When $\sigma_{train} >$ 0.0, the developed EchemNet models performed well on data containing noise at least up to, if not better than, the degree of noise on which they were trained, although in general a larger σ_{train} value decreases the DL model's performance. Balancing the model's performance and noise resistance, EchemNet model with $\sigma_{train} = 0.01$ was selected as the default baseline model whose performance does not decrease significantly until $\sigma_{test} \geq 0.05$. As illustrated by the exemplary simulated voltammograms (Fig. S3), a noise tolerance towards $\sigma_{test} < 0.05$ is deemed sufficient for typical electrochemistry experimentalists.

We further evaluated EchemNet's sensitivity towards small redox features in multi-redox voltammograms. We evaluated the distribution of *fn* events, cases when known redox events

were not detected, as a function of a dimensionless scaling factor S_z that semi-quantifies the corresponding redox z's relative intensity (in terms of current density) against the strongest one within a multi-redox voltammogram (Fig. 5E, Supplementary Note 4). While the S_z values within the training set are uniformly distributed between 0.2 and 1.0 with an average of 0.6, the S_z values in *fn* cases may deviate from such a uniform distribution and will illustrate how the magnitude of redox peak intensities affects DL performance (Fig. 5E). Fig. 5F illustrates how the S_z distribution of *fn* events ($\sigma_{train} = 0.01$) is affected by the degree of noise in the test data (σ_{test}), by displaying each distributions' average (dark blue), medium (red), the first and third quartiles (lower and upper bound of the box) of S_z values. Compared to the test set, S_z's averages among *fn* events are significant lowers and *fn* events' distributions skew towards smaller S_z values. This suggests that statistically EchemNet is more likely to miss smaller redox features during object detection, although those *fn* events are only about 3% of all tested cases ($\sigma_{train} = \sigma_{test} = 0.01$). As σ_{test} increases, the *fn* events' distribution initially shifts towards smaller S_z values when $\sigma_{test} \leq 0.05$, suggesting that larger noise renders small redox features more challenging to detect. Interestingly under sufficient large σ_{test} values ($\sigma_{test} \geq 0.05$) the *fn* events' distribution reversed to better align with the overall S_z distribution in the training set, indicating that the data had reached a noise level where all events were equally difficult to detect. Presumably benefiting from the 1D adaptation of Faster R-CNN architecture that only considers voltage in redox-event detection, our developed EchemNet is capable of detecting small redox features, tested down to $S_z = 0.2$ (20% of the maximal redox feature) in our case, and remains sensitive enough as long as $\sigma_{test} \leq 0.05$.

DISCUSSIONS

Our results shown above demonstrate the technical feasibility of a DL model that detects and analyzes multiple redox features in multi-redox cyclic voltammograms with minimal *a priori* knowledge. Following previous works from our group and others that classify a pre-defined single-redox's mechanism, [11, 12] this work advances and expands the capability of multi-redox detection and classification, mimicking manual analysis that has been prevalent in the past several decades. Given the foundational role of cyclic voltammetry in electrochemistry, an automated DL model for analyzing cyclic voltammograms will transform how electrochemical data will be analyzed in the future. In the following discussions, we provide our reckoning over multiple related issues, in an effort to guide the future development of DL models not only for cyclic voltammetry but also for electrochemistry in general.

The DL model can be slightly, at least, extended for the analysis of new mechanistic scenarios that the model has not seen before during the training process. The simulated multi-redox voltammograms in the training set presume independent redox events, which do not interfere with each other (Supplementary Note 2) and are sufficiently separated in redox potentials (Supplementary Note 4). Yet the deployment of DL model in both $Co^{II}TPP$ and nitroxyl derivative systems (Fig. 4) hints that the DL model can be deployed with satisfactory outcomes to systems with sequential redox events on the same chemical species. When the redox events of the same redox species are sufficiently separated in voltage, the local concentration profiles for one redox event within the solution's diffusion layer shall not be affected by the history of preceding redox processes. This justifies that our DL model can be applied to well-separated redox processes of the same chemical species. Indeed, the correct detection and classification in Fig. 4K showcases the EchemNet is tolerant to large deviations from the training set. Nonetheless, to what extent strongly correlated redox features in close voltage proximity can be analyzed by DL model remains to tested. Such knowledge will prove beneficial in an attempt to develop the DL model's capability of establishing correlation/causality among redox events, one critical feature in manual inspection of voltammograms.

The DL model is considered robust against noises and smaller redox features. Our analysis in Fig. 5 suggests that the DL model can tolerate extensive degrees of Gaussian noises, as long as the training set contains similar levels of noises. What is interesting is that the extent of tolerable noise (σ_{test}) can be slightly larger than the noise during the training process (σ_{train}) (Fig. 5B to 5D), suggesting that the DL architecture per se is pretty resistant against noises. Similar robustness is observed towards the magnitude of current density (i) of the redox feature, in this work represented as the dimensionless factor S_z. Although Fig. 5F suggests that smaller redox features are more prone to be missed during redox-event detection (*fn* cases), the effect is relatively mild and highly dependent on the extent of noise in the dataset. This presumably illustrates the benefits of our 1D adaptation of the DL architecture, which only consider a redox's voltage window and presumably minimizes the possible bias towards large redox features. Although our existing dataset of simulated voltammograms ensures sufficiently separation among redox events (Supplementary Note 4), one venue of future research is to examine and potentially improve the sensitivity of detecting small redox events in close proximity with big redox features, a frequently encountered challenge in manual inspection of voltammograms. As credible experimental data are not expected to be significantly noisy (say, $\sigma < 0.02$), the developed DL model is presumed sufficient towards smaller redox features in the voltammograms.

One interesting issue that we discovered during our research is the quantitative descriptors to store the information of electrochemical potentials for a specific redox process. Our recent efforts in DL analysis of voltammograms[8, 12] suggest that the mechanism propensity vector **y** serves well as the descriptor for mechanism classification in a probabilistic manner. What is challenging is how to describe the "voltage window" in which a certain redox process takes place. While molecular electrochemistry tends to use peak potential, mid-point potential, and/or half-wave potential from voltammograms to describe redox features, [2, 3, 5] such descriptors are not applicable to redox processes when a well-defined voltammetric peak is not available (say, T mechanism). Indeed, it is common in electrochemistry that the smooth voltammetric curves with commonly overlapping redox events render vague definition of a "voltage window" (just consider the term "onset potential"). As detailed in Supplementary Note 4, one innovation of this work is our own definition of a "voltage window" (E_{low} and E_{high}) following a practical yet a bit arbitrary protocol. At present, our devised descriptors E_{low} and E_{high} seem satisfactory based on our manual inspection within simulated and experimental data.

Our work highlights the necessity of a database composed of experimental cyclic voltammograms. Although the simulated training set for the DL model benefits from the exhaustive sampling of mechanisms' parameter space, it remains critical to introduce experimental data during the model's training, evaluation, and future refinement processes. The confusion matrix (Fig. 3C) illustrates that EC_a, EC_b and *DISP-1* mechanisms are more challenging than others for the DL model

to categorize. We propose to use experimental data to address the model's "confusion" among those 3 mechanisms. The low values of *E* mechanism's propensity (y_E) for $Co^{II}TPP$ (79.1% in Fig. 4E) and nitroxyl derivatives (75.4% and 75.8% in Fig. 4H and 4I, respectively) are another concerning point, as we had expected much larger y_E values for those classical quasi-reversible electron transfers. While simulated voltammogram of *E* mechanism precludes any side reactions, experimentally it is likely to have trace side reactions, for example from impurities or trace moisture in anhydrous solvents, which may slightly deviate voltammograms from theoretical ones. Thus the DL model trained by simulated voltammograms is deemed too restrictive on the conditions of an *E* mechanism, and it is necessary to use experimental data to further refine the model.

One challenge for future development of DL model in electrochemistry is the absence of any datasets with annotated ground truths of "voltage windows" and mechanism assignments. In the research field of image recognition, multiple public datasets of $10^3 \sim 10^7$ curated real-life images are available for researchers to test, evaluated, and improve their developed models. [26, 27] Historically, such publicly available datasets greatly propelled the development of DL models for image recognition. Yet to date there is not such an equivalent dataset available for the electrochemistry community. We hypothesize that a well-curated dataset of electrochemical characterizations will have a similar effect over the research of artificial intelligence in electrochemistry. Such an effort is currently undergoing. In the future, we envision a hybrid approach of model development, by feeding both simulated and experimental data during the training/refinement processes.

Finally, we note EchemNet's potential broader impacts towards the research community of electrochemistry and beyond. The development of DL model that automates electrochemical mechanistic analysis does not obviate human researchers and experts' opinion in mechanistic studies. Instead, the DL model shall be deemed as a "virtual assistant" that augments the productivity of human researchers, especially when combined with automated experimentation platforms as showcased in our recent demonstration of autonomous closed-loop electrochemical research. [28] The developed DL model does not possess any *a priori* information such as chemical insights. It is critical for human researchers to "inject" such *a priori* knowledge at certain moment during a research investigation to decide the direction of future experiments even with automated experimentation. Last, we emphasize the proper deployment of our developed DL model under sufficient trained human users, which will broaden and facilitate mechanistic investigations in electrochemistry in the long run.

CONCLUSION

In this work, we demonstrated the feasibility of a DL model to detect and analyze redox features in multi-redox voltammograms. We developed a custom-designed Faster R-CNN architecture that tailors to the 1D data format in electrochemical characterizations. Furthermore, we evaluated the DL model's performance against simulated and some exemplary experimental voltammograms. Such an EchemNet model aligns well with the need of data analysis in a general-purpose autonomous electrochemistry platform, which is expected to automatically analyze experimentally measured data on-the-fly with little if any *a priori* knowledge of the chemical system and transduce the available finite information from the analytic results into a decision-making process for the next robotic experiment execution. The EchemNet model's capability of detecting an arbitrary number of redox events is commensurate with a data analysis process that accommodates a wide range of redox events, expected or unexpected, with little if any *a priori* chemistry knowledge. The DL model's probabilistic approach of mechanistic classification avoids deterministic mechanistic assignments, undesired when only finite information is available during the experimental exploration, and allows for decision-making process based on the analyzed propensity distribution. Our EchemNet model will augment the productivity of human researchers.

Additional research is needed in order to achieve the aforementioned functionality in an autonomous electrochemistry platform. In particular, additional deployment of the DL model towards a large dataset of experimental voltammograms with diverse mechanisms is desired to further evaluate if not validate the model's utility in real-life applications. We call for the establishment of a public database of curated experimental voltammograms with a wide range of mechanisms. Such a public database will not only help benchmark future models' performance but also provide the training set for additional model refinement. A synergistic combination of simulated voltammograms that numerically exhaust all possible mechanistic variations and experimental ones that offer the taste of real-life scenarios is hypothesized to yield an artificial intelligence of electrochemical mechanistic deciphering that rivals if not surpass human intelligence.

ASSOCIATED CONTENT

Supporting Information

The Supporting Information is available free of charge at,

Protocols for numerical simulations of cyclic voltammograms; detailed definitions of individual electrochemical mechanisms; protocols for establishing the DL model; methods for the experimental electrochemical data; supplementary figures related to the DL architecture.

AUTHOR INFORMATION

Corresponding Authors

Cyrille Costentin − *Université Grenoble Alpes, DCM, CNRS, 38000 Grenoble, France*; orcid.org/0000-0002-7098-3132; Email: cyrille.costentin@univ-grenoble-alpes.fr

Quanquan Gu − Department of Computer Science, University of California Los Angeles, Los Angeles, California 90095, United States; Email: qgu@cs.ucla.edu

Chong Liu − Department of Chemistry and Biochemistry, and California NanoSystems Institute, University of California Los Angeles, Los Angeles, California 90095, United States; orcid.org/0000-0001-5546-3852; Email: chongliu@chem.ucla.edu

Authors

Benjamin B. Hoar − Department of Chemistry and Biochemistry, University of California Los Angeles, Los Angeles, California 90095, United States

Weitong Zhang − Department of Computer Science, University of California Los Angeles, Los Angeles, California 90095, United States; orcid.org/0000-0003-4731-9986

Yuanzhou Chen − Department of Computer Science, University of California Los Angeles, Los Angeles, California 90095, United States

Jingwen Sun − Department of Chemistry and Biochemistry, University of California Los Angeles, Los Angeles, California 90095, United States; orcid.org/0000-0003-3657-7672

Hongyuan Sheng − Department of Chemistry and Biochemistry, University of California Los Angeles, Los Angeles, California 90095, United States; orcid.org/0000-0002-0494-4418

Yucheng Zhang − The Oden Institute for Computational Engineering and Sciences, The University of Texas at Austin, Austin, Texas, 78712, United States
Jenny Y. Yang – Department of Chemistry, University of California Irvine, Irvine, California 92697, United States; orcid.org/0000-0002-9680-8260

Author Contributions

B.B.H., W.Z., and Y.C. contribute equally to this work. C.L. supervised the project. B.B.H., C.C., and C.L. developed the theoretical computational frameworks for the generation of simulated cyclic voltammograms. Y.Z. provided python scripts for SR mechanism data generation. W.Z., Y.C., and Q.G. established the machine learning architecture. B.B.H. generated and sanitized the data necessary for model training/validation, and evaluated the established machine-learning model. J.S. and H.S. conducted and analyzed experimental voltammograms with the developed model. B.B.H. wrote the initial manuscript draft, C.C. and J.Y.Y provided critical insights, C.L. finalized the manuscript. All of the authors discussed the results of the project and assisted with manuscript preparation.

Notes

The authors declare the following competing financial interest(s): B.B.H., W.Z., Y.C., Q.G., and C.L. have filed a provisional patent for the work reported here.

ACKNOWLEDGMENTS

J.Y.Y., Q.G. and C.L. acknowledge the National Science Foundation (NSF) (CHE-2247426), W.Z. acknowledges the UCLA Dissertation Year Fellowship, C.C. acknowledges the partial support from Agence Nationale de la Recherche (Labex ARCANE, CBH-EUR-GS, ANR-17-EURE-0003). The authors thank Prof. Matthew Sigman and Dr. Avijit Hazra for constructive discussions. C.L. is grateful for the feedbacks from the attendees in the 2023 Telluride Workshop "Molecular Transformation through Proton-Coupled Electron Transfer for Energy Storage and Conversion". C.L. thanks the constructive interactions with "echem", a *Felis catus* at his residence that inspires the naming of EchemNet. (^ↀᴥↀ^)

REFERENCES

(1) Nicholson, R. S. Theory and Application of Cyclic Voltammetry for Measurement of Electrode Reaction Kinetics. *Anal. Chem.* **1965**, *37* (11), 1351−1355. DOI: 10.1021/ac60230a016.

(2) Bard, A. J.; Faulkner, L. R.; White, H. S. *Electrochemical Methods: Fundamentals and Applications*; 3rd edition; John Wiley & Sons, inc., 2022.

(3) Savéant, J.-M.; Costentin, C. *Elements of Molecular and Biomolecular Electrochemistry: An Electrochemical Approach to Electron Transfer Chemistry*; 2nd edition; John Wiley & Sons, Inc., 2019.

(4) Compton, R. G.; Banks, C. E. *Understanding Voltammetry*; 3rd edition; World Scientifiic Publishing Co Pte Ltd, 2018.

(5) Eliaz, N.; Gileadi, E. *Physical Electrochemistry: Fundamentals, Techniques, and Applications*; John Wiley & Sons, Inc., 2019.

(6) Elgrishi, N.; Rountree, K. J.; McCarthy, B. D.; Rountree, E. S.; Eisenhart, T. T.; Dempsey, J. L. A Practical Beginner's Guide to Cyclic Voltammetry. *J. Chem. Educ.* **2018**, *95* (2), 197−206. DOI: 10.1021/acs.jchemed.7b00361.

(7) Britz, D.; Strutwolf, J. *Digital Simulation in Electrochemistry*; Springer, 2016.

(8) Sun, J.; Liu, C. What and how can machine learning help to decipher mechanisms in molecular electrochemistry? *Curr. Opin. in Electrochem.* **2023**, *39*, 101306. DOI: 10.1016/j.coelec.2023.101306.

(9) Gundry, L.; Guo, S. X.; Kennedy, G.; Keith, J.; Robinson, M.; Gavaghan, D.; Bond, A. M.; Zhang, J. Recent advances and future perspectives for automated parameterisation, Bayesian inference and machine learning in voltammetry. *Chem Commun* **2021**, *57* (15), 1855−1870. DOI: 10.1039/d0cc07549c.

(10) Chen, H.; Kätelhön, E.; Compton, R. G. Machine learning in fundamental electrochemistry: Recent advances and future opportunities. *Curr. Opin. in Electrochem.* **2023**, *38*, 101214. DOI: 10.1016/j.coelec.2023.101214.

(11) Kennedy, G. F.; Zhang, J.; Bond, A. M. Automatically Identifying Electrode Reaction Mechanisms Using Deep Neural Networks. *Anal. Chem.* **2019**, *91* (19), 12220−12227. DOI: 10.1021/acs.analchem.9b01891.

(12) Hoar, B. B.; Zhang, W.; Xu, S.; Deeba, R.; Costentin, C.; Gu, Q.; Liu, C. Electrochemical Mechanistic Analysis from Cyclic Voltammograms Based on Deep Learning. *ACS Meas. Sci. Au* **2022**, *2* (6), 595−604. DOI: 10.1021/acsmeasuresciau.2c00045.

(13) Gundry, L.; Kennedy, G.; Bond, A. M.; Zhang, J. Establishing zone regions in cyclic voltammetry using unsupervised machine learning. *J. Electroanal. Chem.* **2023**, *942*, 117551. DOI: 10.1016/j.jelechem.2023.117551.

(14) Chen, H.; Katelhon, E.; Compton, R. G. Predicting Voltammetry Using Physics-Informed Neural Networks. *J Phys Chem Lett* **2022**, *13* (2), 536−543. DOI: 10.1021/acs.jpclett.1c04054.

(15) Chen, H.; Batchelor-McAuley, C.; Kätelhön, E.; Elliott, J.; Compton, R. G. A Critical Evaluation of Using Physics-Informed Neural Networks for Simulating Voltammetry: Strengths, Weaknesses and Best Practices. *J. Electroanal. Chem.* **2022**, *925*, 116918. DOI: 10.1016/j.jelechem.2022.116918.

(16) Chen, H.; Katelhon, E.; Compton, R. G. Rotating Disk Electrodes beyond the Levich Approximation: Physics-Informed Neural Networks Reveal and Quantify Edge Effects. *Anal. Chem.* **2023**, *95* (34), 12826−12834. DOI: 10.1021/acs.analchem.3c01936.

(17) Bishop, C. M. *Pattern Recognition and Machine Learning*; Springer, 2006.

(18) Schachterle, S. D.; Perone, S. P. Classification of voltammetric data by computerized pattern recognition. *Anal. Chem.* **1981**, *53* (11), 1672−1678. DOI: 10.1021/ac00234a028.

(19) He, K.; Zhang, X.; Ren, S.; Sun, J. Deep Residual Learning for Image Recognition. *2016 IEEE Conference on Computer Vision and Pattern Recognition (CVPR)* **2016**, 770−778. arXiv:1512.03385.

(20) Ren, S.; He, K.; Girshick, R.; Sun, J. Faster R-CNN: Towards Real-Time Object Detection with Region Proposal Networks. *Advances in Neural Information Processing Systems 28 (NIPS 2015)* **2015**. arXiv:1506.01497.

(21) Taha, A. A.; Hanbury, A. Metrics for evaluating 3D medical image segmentation: analysis, selection, and tool. *BMC Med Imaging* **2015**, *15*, 29. DOI: 10.1186/s12880-015-0068-x

(22) Lin, T.-Y.; Dollar, P.; Girshick, R.; He, K.; Hariharan, B.; Belongie, S. Feature Pyramid Networks for Object Detection. *2017 IEEE Conference on Computer Vision and Pattern Recognition (CVPR)* **2017**, 2117−2125. arXiv:1612.03144.

(23) Costentin, C.; Passard, G.; Robert, M.; Savéant, J.-M. Concertedness in proton-coupled electron transfer cleavages of carbon–metal bonds illustrated by the reduction of an alkyl cobalt porphyrin. *Chem. Sci.* **2013**, *4* (2), 819−823. DOI: 10.1039/c2sc21788k.

(24) Rafiee, M.; Miles, K. C.; Stahl, S. S. Electrocatalytic Alcohol Oxidation with TEMPO and Bicyclic Nitroxyl Derivatives: Driving Force Trumps Steric Effects. *J. Am. Chem. Soc.* **2015**, *137* (46), 14751−14757. DOI: 10.1021/jacs.5b09672.

(25) Nutting, J. E.; Rafiee, M.; Stahl, S. S. Tetramethylpiperidine N-Oxyl (TEMPO), Phthalimide N-Oxyl (PINO), and Related N-Oxyl Species: Electrochemical Properties and Their Use in Electrocatalytic Reactions. *Chem. Rev.* **2018**, *118* (9), 4834−4885. DOI: 10.1021/acs.chemrev.7b00763.

(26) Deng, J.; Dong, W.; Socher, R.; Li, L. J.; Kai, L.; Li, F.-F. ImageNet: A large-scale hierarchical image database. *2009 IEEE Conference on Computer Vision and Pattern Recognition (CVPR)* **2009**, 248−255. DOI: 10.1109/CVPR.2009.5206848.

(27) Lin, T.-Y.; Maire, M.; Belongie, S.; Hays, J.; Perona, P.; Ramanan, D.; Dollár, P.; Zitnick, C. L. Microsoft COCO: Common Objects in Context. In *Computer Vision – ECCV 2014*, 740−755. arXiv:1405.0312.

(28) Sheng, H.; Sun, J.; Rodríguez, O.; Hoar, B. B.; Zhang, W.; Xiang, D.; Tang, T.; Hazra, A.; Min, D. S.; Doyle, A. G.; et al. Autonomous closed-loop mechanistic investigation of molecular electrochemistry via automation. *chemrxiv* **2023**. DOI: 10.26434/chemrxiv-2023-psqxj.